OXFORD UNIVERSITY PRESS | Human Molecular Genetics

Golgi-retained Cx32 mutants interfere with gene addition therapy for CMT1X

Journal:	*Human Molecular Genetics*
Manuscript ID	HMG-2016-D-01187.R1
Manuscript Type:	2 General Article - UK Office
Date Submitted by the Author:	n/a
Complete List of Authors:	Kyriakoudi, Styliana; The Cyprus Institute of Neurology and Genetics, Neuroscience Laboratory Sargiannidou, Irene; The Cyprus Institute of Neurology and Genetics, Neuroscience Laboratory Kagiava, Alexia; The Cyprus Institute of Neurology and Genetics, Neuroscience Laboratory Olymbiou, Margarita; The Cyprus Institute of Neurology and Genetics, Neuroscience Laboratory Kleopa, Kleopas; The Cyprus Institute of Neurology and Genetics, Neurology Clinics and Neuroscience Laboratory
Key Words:	Inherited neuropathy, gene therapy, gap junctions, Charcot-Marie-Tooth disease, Schwann cells

Golgi-retained Cx32 mutants interfere with gene addition therapy for CMT1X

Styliana Kyriakoudi,[1] Irene Sargiannidou,[1] Alexia Kagiava,[1] Margarita Olympiou,[1] Kleopas A. Kleopa[1,2,*]

[1]Neuroscience Laboratory and [2]Neurology Clinics, The Cyprus Institute of Neurology and Genetics and Cyprus School of Molecular Medicine, Nicosia, Cyprus

[*]**Correspondence**: Prof. Kleopas A. Kleopa, MD

The Cyprus Institute of Neurology and Genetics

6 International Airport Avenue, P.O. Box 23462,

1683, Nicosia, CYPRUS

+357 22 358600

+357 22 392786

kleopa@cing.ac.cy

Abstract

Numerous *GJB1* gene mutations cause the X-linked form of Charcot-Marie-Tooth disease (CMT1X). *GJB1* encodes connexin32 (Cx32), which forms trans-myelin gap junctions in Schwann cells. Most *GJB1* mutations result in loss-of-function mechanisms, supporting the concept of gene replacement therapy. However, interactions between delivered wild type and endogenously expressed mutant Cx32 may potentially occur in the setting of gene replacement therapy. In order to screen for possible interactions of several representative CMT1X mutants with wild type Cx32 that may interfere with functional gap junction formation, we established an *in vitro* screening method co-expressing in HeLa cells wild type Cx32 and one of eight different Cx32 mutants including A39P, A39V, T55I, R75W, M93V, L143P, N175D and R183S. Some of the Golgi-retained mutants hindered gap junction plaque assembly by Cx32 on the cell membrane, while co-immunoprecipitation analysis revealed a partial interaction of wild type protein with Golgi-retained mutants. Dye transfer studies confirmed that Golgi-retained R75W, M93V and N175D but not endoplasmic reticulum-retained T55I had a negative effect on wild type Cx32 function. Finally, *in vivo* intraneural delivery of the gene encoding the wild type Cx32 in mice bearing either the T55I or R75W mutation on Cx32 knockout background showed that virally delivered protein was correctly localized in mice expressing the endoplasmic reticulum-retained T55I whereas it did not traffic normally in mice expressing the Golgi-retained R75W. Thus, certain Golgi-retained Cx32 mutants may interfere with exogenously delivered Cx32. Screening for mutant-wild type Cx32 interactions should be considered prior to planning gene addition therapy for CMT1X.

Introduction

Charcot-Marie-Tooth (CMT) disease is one of the commonest inherited neurological disorders causing progressive degeneration of the peripheral nervous system (1) affecting approximately 1 in 2500 individuals worldwide. The X-linked form of the disease is one of the most common among all types of CMT and is caused by over 400 different mutations in the *GJB1* gene distributed throughout its length (http://hihg.med.miami.edu/code/http/cmt/public_html/index.html#/) (2, 3). The *GJB1* gene encodes for connexin32 (Cx32), a transmembrane protein which forms gap junctions (GJs) in non-compact myelin areas in myelinating Schwann cells and oligodendrocytes (3-5). GJs are formed by hexamers of connexin proteins at specialized regions of the plasma membrane allowing diffusion of metabolites, ions and electrical impulses (6). The exchange of such essential substances between cells or between different compartments of the same cell as in the case of myelinating Schwann cells is crucial for preservation of homeostasis, cell survival and function (7, 8). CMT1X patients are characterized by demyelination and length-dependent degeneration of peripheral nerves which result in progressive distal muscle weakness and wasting, foot deformities, areflexia and sensory deficits (9, 10).

Most of the CMT1X mutations are thought to cause loss of Cx32 function as they lead to a phenotype that does not differ from the one resulting from complete deletion of the *GJB1* gene (11-15). Many Cx32 mutants have been studied *in vitro* and showed abnormal trafficking and intracellular retention in the endoplasmic reticulum (ER) and/or Golgi (16-20) followed by proteasomal or lysosomal degradation (21). Other mutants may traffick to the membrane, but form non-functional channels or channels with altered biophysical properties (22-24). In the case of most Cx32 mutants, lack of GJ formation or formation of GJ channels with altered activity ultimately leads to loss of GJ function in Schwann cells. This loss of function leads to disturbance

of homeostasis not only in Schwann cells and the myelin they form, but also in axons through impaired axonal transport and signaling (25-28).

Early *in vitro* studies indicated that some of Cx32 mutants may also exert dominant negative effects on the co-expressed wild type (WT) protein (11, 17) while *in vivo* models have demonstrated a possible interference of endogenously expressed Cx32 mutants with the WT Cx32 when co-expressed transgenically in the same cells. In particular, the R142W (29) and R75W (12) mutants, both retained in the Golgi, but not the ER-retained T55I mutant, reduced the expression of co-expressed WT Cx32. The interference of some CMT1X mutants with the WT protein occurring in experimental models is not clinically relevant for this X-linked disease at baseline given that one of the *GJB1* alleles is always inactivated (in women), or only one is present (in men). However, it may impair future gene replacement approaches using viral vectors recently developed (30, 31) when trying to introduce the WT gene into cells that also express the mutants.

To examine whether a number of different Cx32 mutants could exert any dominant negative effect on the co-expressed WT protein we performed an *in vitro* screening assay. We examined the cellular expression of eight different missense mutations associated with CMT1X and their possible interactions with the co-expressed WT Cx32 protein, including the ER-retained A39P, A39V and T55I and the Golgi-retained R75W, M93V, L143P, N175D and R183S mutants. We have also investigated these effects *in situ* by intrasciatic injections in Cx32 KO mice expressing either the T55I or the R75W mutant on a Cx32 KO background, designated as T55I KO and R75W KO, respectively, which are representative of the CMT1X mutations. Our results suggest that none of the ER-retained mutants impair the correct trafficking of Cx32 hemichannels to cell membrane while some of the Golgi-retained mutants show a partial interaction with the virally delivered WT Cx32. Thus, they may potentially interfere with future gene delivery in patients bearing these mutations. Our study also provides quick screening tools for determining which

CMT1X mutants could interact with virally delivered Cx32, prior to planning future gene therapy approaches.

Results

Golgi-retained CMT1X associated mutants impair the trafficking of WT Cx32 to the cell membrane *in vitro*

In order to examine whether Cx32 mutants could have a dominant negative effect on co-expressed WT Cx32 by impeding the normal trafficking to the cell membrane, we studied the cellular effects of eight pathogenic missense mutations of Cx32. These were selected because their *in vitro* intracellular retention in the ER (A39P, A39V, T55I), or Golgi (R75W, M93V, L143P, N175D and R183S) is representative of most CMT1X mutations (19, 20, 32). The localization of each mutant when expressed in communication-incompetent HeLa cells and its capacity to form GJ plaques was first examined by performing immunostainings for Cx32 and markers of the ER (calnexin), Golgi (58k) (**Suppl. Figs. 1 and 2**) or the cell membrane (cadherin) (**Suppl. Fig. 3**). **Table 1** summarizes the intracellular localization of the Cx32 mutants studied and their ability to form GJ plaques.

To assess whether CMT1X mutants could interfere with WT Cx32, we co-expressed by transient transfection the WT Cx32 and each of the eight mutants in HeLa cells. We performed immunostaining against the flag tag to specifically label the WT Cx32 and myc tag to specifically label the mutant Cx32 protein (**Fig. 1A-I, Suppl. Fig. 4**). Overall, the WT protein appeared to form many GJ plaques on the cell membrane of cells co-expressing most CMT1X mutants similar to cells expressing the WT Cx32 alone. However, WT protein appeared to be mostly

intracellularly retained in cells expressing the R75W mutant, and partly retained in cells expressing the M93V and N175D mutants. Counts of the number of GJ-like plaques formed on the cell membrane of double expressing cells, demonstrated that most mutants did not cause a significant inhibition of the correct trafficking of the WT Cx32 and formation of GJs on the cell membrane. However, two of the Golgi retained mutants, the R75W and N175D caused a significant reduction of GJ plaques formed by WT Cx32 in co-expressing cells ($p<0.001$ and $p=0.00608$, respectively) as compared to the number of GJ plaques formed in cells expressing only the WT Cx32, suggesting dominant negative effects (**Fig. 1J**).

To further confirm the expression of the myc-tagged Cx32 mutants and the flag-tagged WT Cx32, we examined their levels in double transfected cells by immunoblot analysis. This experiment confirmed the presence of both myc-tagged mutants and flag-tagged WT Cx32, mostly at comparable levels although in some experiments the level of the mutant or the WT protein was higher, without correlation to the presence or not of dominant effects. In non-transfected HeLa cells there was complete absence of immunoreactivity with either the flag or myc antibody, while the absence of a myc band in cells transfected only with the WT protein and an empty plasmid, confirmed the expression of the WT protein only, in those cells **(Fig. 2)**.

Golgi-retained CMT1X mutants interact directly with co-expressed WT Cx32

To further clarify the nature of dominant negative effects of some CMT1X mutants, we assessed whether there is any direct interaction between the mutants and the WT protein. Such interaction could be a plausible explanation for dominant negative effects since during the folding and oligomerization of connexins into hexamers taking place after exiting the ER in the ER - cis Golgi network (33, 34), mutant connexins could participate in the same hexamer oligomerizing with WT protein monomers. This interaction could prevent the trafficking of the entire hexamer including WT Cx32 to the cell membrane and impair the formation of functional GJ channels. In

this experiment, we co-transfected HeLa cells with the WT protein fused to a flag tag along with the myc-tagged mutants and performed co-immunoprecipitations. This analysis showed that none of the ER-retained mutants interacted with the WT protein, while three of the Golgi-retained mutants, the R75W, M93V and N175D, revealed a partial interaction (**Fig. 3A**). Nevertheless, the interaction level of the R75W, M93V and N175D with the WT protein was lower compared to the WT-WT interactions (**Fig. 3B**). Notably, when we co-expressed the WT flag-tagged protein with the WT myc-tagged Cx32, a strong band on the immunoblot confirmed their full interaction, as expected from the formation of hexamers before reaching the cell membrane.

Functional impairment of GJ connectivity in cells co-expressing WT Cx32 with the R75W, M93V, and N175D but not with the T55I mutant

Given the interference of some Golgi-retained Cx32 mutants with the normal trafficking of the co-expressed WT Cx32 shown with the immunocytochemistry and the direct interaction shown by immunoprecipitation, we then asked whether these interactions could also affect the function of GJ channels formed by the WT Cx32. To investigate this possibility, we examined four representative mutants, the Golgi-retained R75W, M93V and N175D mutants, which showed interaction with the WT protein, and the ER-retained T55I that did not interact. These mutations were cloned along with the dsRED fluorescent marker as a reporter gene and co-expressed with the WT protein which was traced by the eGFP. Possible impairment of GJ channel function was assessed by Lucifer yellow scrape loading assay with quantification of coupled cells co-expressing WT Cx32 and each of the four mutants (**Fig. 4A-P**). Our results demonstrated no significant functional impairment of GJ connectivity in cells co-expressing WT Cx32 and the ER-retained T55I mutant ($p>0.05$), whereas a significant reduction of coupled cells was observed in the presence of the R75W ($p=0.0001$), M93V ($p=0.00055$) and N175D ($p=0.0063$) mutants, compared to the coupled cells expressing only the WT Cx32 (**Fig. 4Q**).

Thus, our *in vitro* results suggest a direct interaction of at least three of the Golgi-retained mutants with the WT Cx32 when co-expressed in the same cells, leading to reduced formation of GJ plaques on the cell membrane by WT Cx32, and reduced cell coupling, while such interactions were not observed with ER-retained mutants.

Intraneural *GJB1* gene delivery leads to WT Cx32 expression and correct localization at paranodal non-compact myelin areas in T55I KO but not in R75W KO sciatic nerves

In order to confirm the correct trafficking of the WT Cx32 in the presence of a mutant protein in myelinating Schwann cells *in vivo*, we performed intraneural injections of the LV.*Mpz-GJB1* (full) or LV.*Mpz*-eGFP (mock) vector directly into sciatic nerves of 2-mo-old T55I KO and R75W KO mice, as well as simple Cx32 KO (*Gjb1*-null) mice, as controls. The human *GJB1* gene expression is driven specifically in myelinating Schwann cells by the rat myelin protein zero (*Mpz*) promoter (30, 35). Cx32 expression and localization was analyzed 4 weeks post injection by immunostaining of teased fibers from injected nerves. Double immunostaining for Cx32 and the paranodal marker Caspr revealed Cx32 immunoreactivity only in the perinuclear cytoplasm of Schwann cells in T55I KO nerves injected with the mock vector, representing the endogenous mutant Cx32 (**Fig. 5A**). In contrast, T55I KO nerves injected with the full vector (LV.*Mpz-GJB1*) showed in addition to the perinuclear mutant Cx32 immunoreactivity, also correct Cx32 localization at paranodal non-compact myelin areas where Cx32 is normally expressed (4), representing the virally expressed WT Cx32 (**Fig. 5B**). The expression of virally delivered WT Cx32 in T55I KO nerve fibers was similar to the expression obtained in control Cx32 KO mice that did not express any Cx32 endogenously, injected with the same vector. On the other hand, Cx32 immunoreactivity was absent at most paranodal myelin areas in the R75W KO sciatic nerve fibers injected with the full vector (**Fig. 5C**). Additionally, mutant Cx32 was highly expressed in the perinuclear Schwann cell cytoplasm, indicating retention of the R75W mutant, likely together with the exogenously expressed WT protein.

Counts from randomly selected paranodal areas revealed that there was no significant difference in the percentage of Cx32-positive paranodal areas between T55I KO and Cx32 KO nerves injected with the full vector ($p>0.5$; n=50 nodal areas per mouse, n=8 mice per genotype), indicating that the T55I mutant does not inhibit the correct trafficking of the virally delivered WT Cx32 and correct localization at paranodal areas *in vivo*. In contrast, a significant reduction of Cx32-positive paranodal areas was found in full vector injected R75W KO nerve fibers compared to full vector injected Cx32 KO nerves ($p=0.00011$; n=50 nodal areas per mouse, from n=4 mice), confirming that the R75W mutant likely exerts dominant negative effect on the virally delivered WT Cx32 protein causing largely cytoplasmic retention in myelinating Schwann cells *in vivo* (**Fig. 5D**), in keeping with our *in vitro* results.

Discussion

This study provides insights into possible interactions between Cx32 mutants associated with CMT1X and the co-expressed WT Cx32, with important implications for future gene therapy approaches to treat patients suffering from this disease. Our *in vitro* and *in vivo* studies show a differential effect of several Cx32 mutants, with Golgi-retained mutants showing the highest likelihood for dominant negative effects. Methods developed in this study could provide a screening tool for rapid testing of further CMT1X mutants for possible interactions when gene replacement therapy is considered.

Previous studies have shown that Cx32 mutants often accumulate intracellularly, localizing predominantly in the ER or Golgi with or without the formation of rare GJ-like plaques (17, 19, 20). As misfolded proteins could be toxic for the cell, they are degraded efficiently via lysosomal or proteasomal protein degradation pathways (21). In keeping with previous studies in which the

expression of most of these mutants has been examined, we show here that the A39P, A39V and T55I mutants were retained primarily in the ER whereas the R75W, M93V, L143P, N175D and R183S mutants co-localized with the 58k Golgi marker. Some of the mutants showed additional localization in cytoplasmic vesicles (M93V, N175D, R183S). HeLa cells expressing only the WT Cx32, which served as a positive control, exhibited distinct and large GJ plaques at the intracellular boundaries of apposed membranes while Cx32 expression was also sometimes detectable as a punctuate pattern in the cytoplasm due to its high expression. The M93V and R183S mutants exhibited mostly cytoplasmic pattern with rare GJ plaques at intercellular contact regions compared to the WT Cx32, whereas the A39P, A39V, T55I, R75W and L143P and N175D exhibited exclusively a cytoplasmic expression pattern. The CMT1X mutants examined here are therefore representative of most other Cx32 mutations reported and previously expressed *in vitro* or *in vivo* (12, 19, 20, 29).

In the present study, we have examined the localization of eight Cx32 gene mutants discovered in CMT1X patients and investigated their possible interference with the WT protein. For this purpose, each mutant was co-expressed with the WT protein in HeLa cells and assessed for GJ-like plaque formation on the cell surface. Our immunofluorescence data revealed that when co-expressed with the R75W and N175D mutants, the WT protein was partially retained intracellularly and failed to reach the cell membrane. Furthermore, co-immunoprecipitation assay revealed that the three Golgi-retained mutants R75W, M93V and N175D exhibited a direct interaction with the WT protein whereas the remained five mutants did not demonstrate such interaction. Any differences in the expression levels of the mutant and WT proteins did not affect our immunostaining results, as in our analysis we included individual cells co-expressing both the WT and mutant protein.

Moreover, our functional assay tracing the diffusion of the GJ-permeable tracer Lucifer yellow in cells co-expressing the WT protein with either the ER-retained T55I or the Golgi-retained R75W, M93V and N175D mutants showed that there was a significant reduction of GJ-coupled cells in R75W, M93V and N175D expressing cells, as compared to cells expressing only the WT protein. This indicated a reduced formation of functional GJ channels, whereas in the case of the T55I mutant, Lucifer yellow was transferred to adjacent GJ-coupled cells as expected, suggesting physiological GJ permeability. Further dominant negative effects between co-expressed WT and mutant Cx32 could occur at the functional level once hemichannels with mutant-WT hexamers reach the membrane (18). Although we have not directly tested this possibility in this study, our dye transfer analysis in the scrape loading assay indicates that the M93V mutant, which reaches the cell membrane co-localizing with WT Cx32 as shown by our immunocytochemistry results, could actually impair functional GJ formation and cell connectivity if it participates in the same hemichannels as WT Cx32.

Analysis of possible interactions between WT and mutant Cx32 *in vivo*, demonstrated that the R75W mutant, which also exhibits an interaction with the WT protein *in vitro*, interferes with the WT protein and inhibits its trafficking to the paranodal areas of Schwann cells, where it is normally localized (4). This is in keeping with our previous observations when the R75W mutant was transgenically expressed in WT mice and caused impaired expression of endogenous WT Cx32 as well as mild neuropathy on a WT background (12). In contrast, the T55I mutant did not affect the physiological routing of the WT protein to paranodal areas, as compared to Cx32 KO mice that were injected with the same vector. Thus, our *in vivo* findings correlate with the *in vitro* results showing an interaction of the WT Cx32 at least with the Golgi-retained R75W mutant and not with the ER-retained T55I.

The pattern of interference of the Golgi but not ER-retained mutants with WT Cx32 as shown by this study, is probably attributed to the fact that the ER-retained Cx32 mutants, considered as incorrectly folded proteins, are rapidly degraded in the proteasomes by the ER-associated degradation process (19, 21, 36). In contrast, mutants which can overcome the ER quality control system are further transported to the Golgi, where connexin oligomerization into hexamers takes place (37) before transport to the membrane. In the Golgi apparatus, such mutants may have a direct physical interaction with WT Cx32 molecules during oligomerization events through participation in the same hexamer as shown by our co-immunoprecipitation results. Ultimately, this interaction could disrupt the trafficking of the WT protein to the cell membrane resulting in reduced formation of functional GJ channels. Oligomerization of compatible subunits into hexameric hemi-channels is subject to a strictly regulated process (38, 39). Specific signals could possibly be responsible for the determination of WT-mutant connexin polypeptides compatibility, in analogy to the hetero-oligomerization of different connexin isoforms which is based on specific intrinsic signals. Even a single point mutation could prevent the binding of modifiers that assist the correct folding of a polypeptide and facilitate its interaction with other monomers during oligomerization, or change its surface structure resulting in subunit incompatibility (33). This could be the case for the two Golgi-retained L143P and R183S mutants that did not show any interaction with the WT protein.

One limitation of our study is that the *in vitro* HeLa cell system cannot fully reproduce the *in vivo* conditions, and variations in WT/mutant expression levels may influence some of the results. Although we only examined here a small fraction of the large number of known CMT1X mutations, they are representative of the most common cell expression patterns. Nevertheless, this *in vitro* screening provides a valuable technique to rapidly evaluate the expected efficacy of gene replacement therapy in patients harboring specific CMT1X mutations. Another concern is that the expression rates of the WT and mutant proteins were similar in most *in vitro* experiments

resulting in partial interactions of some Golgi-retained mutants, whereas gene replacement approaches studied so far *in vivo* resulted in lower expression levels of virally delivered Cx32 compared to the endogenous physiological expression levels (30, 31). Likewise, if patients have a higher level of the endogenously expressed interfering mutant compared to virally delivered WT Cx32 dominant negative effects may be maximized abolishing any possible therapeutic benefit. However, this possibility does not limit the validity of our results obtained *in vitro* as they correlate highly with our *in vivo* findings in terms of identifying mutants interacting with WT Cx32. Finally, even though scrape loading assays have been widely used to study GJ function, more sensitive methods such as electrophysiological studies could be used to evaluate GJ conductance more accurately in the setting of WT/mutant Cx32 interactions (40, 41).

Based on the findings of this study that some of the Golgi-retained mutants interfere with the WT Cx32, gene therapy approaches using gene addition may have to be modified for patients harboring mutations with dominant-interfering effects. In such cases, gene editing approaches to correct the specific mutation (42) or RNA interference could be used to downregulate the expression of the mutant allele prior to gene addition of the WT gene (43), or allele-specific silencing (44, 45) should be attempted simultaneously with WT gene addition. For patients harboring ER-retained mutants that do not interfere with WT Cx32, our results suggest that gene addition approaches could be directly performed. The development of such therapeutic approaches has been also supported by animal studies demonstrating restoration of the WT Cx32 protein expression in Schwann cells either by intrathecal (31) or intraneural injections (30) in *GJB1*-null mice.

In conclusion, this study has delineated the possible interactions of eight representative missense *GJB1* mutations with the WT Cx32 protein *in vitro* by investigating intracellular trafficking, direct interactions and GJ function. Moreover, *in vivo* studies confirmed the *in vitro* findings for

two representative mutants. Taken together, the results of this study suggest that the examination and elucidation of possible interactions between the WT Cx32 and each mutant may assist future gene therapy for CMT1X. The extremely large number of mutations reported in the *GJB1* gene to date and their variable cellular-molecular mechanisms mandates a mutation-tailored therapeutic strategy for each individual patient with CMT1X following a prior screening of the mutant effects.

Materials and methods

WT and mutant Cx32 expression constructs

For the *in vitro* co-expression and co-immunoprecipitation experiments, the WT Cx32 was fused to a flag tag in order to examine any possible interactions with the myc-tagged mutants. To insert the flag sequence in the pEGFP-N1 plasmid carrying the *GJB1* ORF, the plasmid was double digested with appropriate enzymes (BamHI/NotI) to remove the eGFP sequence. Specifically designed primers carrying the entire flag sequence with sticky ends (Primer #1: 5 '-GAT CCC GAC TAC AAG GAC GAC GAC GAC AAG TAAGC -3' and Primer #2: 5' –GGC CGC TTA CTT GTC GTC GTC GTC CTT GTA GTC GG -3') were used and the PCR product was ligated into the pEGFP-N1 plasmid. Correct assembly of the expression cassettes was confirmed by restriction digest mapping and direct sequencing.

To distinguish the WT from mutant Cx32 in co-expression experiments, the *GJB1* mutations A39V, A39P, M93V, L143P and R183S were introduced into the WT human Cx32 cDNA (cloned into the pEGFP-N1-Myc plasmid) by polymerase chain reaction using the QuikChange II XL Site-Directed Mutagenesis Kit (Stratagene, USA). For the generation of the mutants,

specifically designed oligonucleotide primers were used to introduce the point mutation as shown on **Table 2**. In the PCR reaction, the high fidelity *Pfu Ultra* DNA polymerase (2.5 U) was used and the PCR products were digested with the DpnI restriction enzyme to eliminate the parental supercoiled DNA. The DpnI-treated DNA was used to transform the XL10-Gold ultracompetent bacterial cells. DNA isolation was performed from single colonies and the *GJB1*/Cx32 sequence for each mutant was confirmed by direct sequencing. The T55I and R75W mutations were taken from previously described constructs (12) while the N175D mutation (obtained from Dr. Donglin Bai, University of Western Ontario) was directionally cloned into the pEGFP-N1-Myc plasmid using the XhoI/BamHI sites.

Lentiviral expression constructs

For the scrape loading assay, the *GJB1* gene along with the downstream internal ribosome entry site (IRES) and eGFP sequence, was PCR amplified from the pIRES2-EGFP-CX32 plasmid using specifically designed primers that introduce the AgeI and SalI restriction sites (Primer #1: 5'- AAA CCG GTG GCA GGA TGA ACT GGA CAGG -3' and Primer #2: 5'- ACG CGT CGA CCC GTT ACT TGT ACA GCT CGT -3'). The PCR product was run on a gel to confirm the correct size band and purified using the Qiagen Gel Extraction Kit (Qiagen, Hilden). The DNA fragment was then directionally cloned into the 2nd generation pCCLsin.PPT.hPGK.GFP.pre lentiviral transfer vector (30) (gift from Dr. Carsten Lederer) under the expression of the ubiquitous *PGK* promoter, following digestion with the AgeI and SalI restriction enzymes. Correct assembly of the expression cassette was confirmed by direct sequencing.

For the *in vivo* intrasciatic injections, the LV.*Mpz-GJB1* expression cassette was produced based on the same lentiviral vector. For this purpose, the human *PGK* promoter was replaced by the rat *Mpz* promoter which is expressed specifically in myelinating Schwann cells (35). The human

GJB1 ORF was inserted downstream of the *Mpz* promoter using appropriate restriction enzymes, along with the IRES and eGFP, serving as a reporter gene. An LV.*Mpz*-eGFP mock vector cassette without the *GJB1* ORF was also cloned to be used as a negative control. Correct expression cassettes were confirmed by direct sequencing of the ORFs.

Lentiviral vector production and titration

Recombinant lentiviruses were produced by co-transfection of the transfer vector with the helper plasmids (CMVΔR8.74, pRSV-Rev, and pMD2-VSVG [vesicular stomatitis virus G protein]) in HEK 293T cells using the calcium phosphate co-precipitation method as previously described (30). Approximately 24 hours prior the transfection, a total of 5 x 10^6 293T cells were seeded in 10 cm plates in Iscove Modified Dulbecco's Medium (IMDM) supplemented with 10% heat inactivated Fetal Bovine Serum (FBS), penicillin and streptomycin (100 U/ml) and glutamine. The plates were incubated O/N in a humidified atmosphere with 5% CO_2 at 37°C. One hour prior to transfection, the culture medium in the plates was removed and replaced with fresh medium. The plasmid DNA mix was prepared by combining 2μg of the envelope plasmid pMD2-VSVG, 20μg of the packaging plasmid CMVΔR8.74, 10μg of the pRSV-Rev and 20μg of the transfer vector plasmid. Then, 521μl of 0.1x TE/dH_2O (2:1) was added to the mixture followed by addition of 60μl 2.5M $CaCl_2$ for 5 minutes. The precipitate was formed by dropwise addition of 600μl 2x HSBSs solution (HEPES-buffered saline) to the mixture while vortexing at full speed. The precipitate was immediately added to the cells and the medium was replaced after 12 hours with fresh medium containing 1mM sodium butyrate. After two days, lentivirus was harvested, cleared by low-speed centrifugation and filtered through a 0.45 μm-pore-size filter. The filtered supernatant was then concentrated using the Lenti-X Concentrator (Clontech, USA) reagent followed by a short incubation and centrifugation. Viral titers were determined by a HIV-1 Gag p24 enzyme-linked immunosorbent assay (ELISA) and quantitative reverse transcription polymerase chain reaction (RT-PCR) for EGFP.

Cell culture and transfections

Communication-incompetent HeLa cells were cultivated in a humidified atmosphere containing 5% CO_2 at 37°C in low-glucose Dulbecco's Modified Eagle's Medium (DMEM) (GIBCO, Invitrogen) supplemented with 10% FBS, antibiotics-antimycotics (penicillin/streptomycin) at a concentration of 100 µg/ml and 10% non-essential amino acids. Cell cultures were routinely subcloned by trypsinization and medium was changed every 2-3 days. Cell transfections were performed using the cationic lipid based Lipofectamine LTX with PLUS reagent transfection system (Invitrogen) when the cells reached approximately 70% confluency. For transient transfection, plasmid DNA (WT or mutant) along with the PLUS reagent and lipofectamine LTX were incubated separately in OptiMem (Reduced-Serum Medium) and then mixed for 15 minutes at RT. The DNA-lipid complex was added dropwise to the cells that were incubated in 4-chamber slides or 6-well plates. The following day, the transfection reagent was replaced with fresh medium.

Immunocytochemistry

Transfected cells were plated on glass slides reaching 90% confluency, fixed in 4% paraformaldehyde (PFA), washed in PBS and permeabilized in acetone for 10 min at -20°C. The slides were then immersed twice in PBS to remove residual acetone and the cells were blocked in blocking solution (5% BSA with 0.1% Triton-X) for 1 hour at RT. Primary antibodies diluted in blocking solution including rat anti-flag (1:100, Biolegend), goat anti-Cx32 (1:300, Santa Cruz) and mouse anti-myc (1:300, Santa Cruz), anti-cadherin (1:500, Abcam), anti-calnexin (1:50, Abcam) and anti-58k (1:50, Abcam) were used and incubated overnight at 4°C. The following day, cells were washed 3x in PBS followed by addition of appropriate fluorescein- and rhodamine-conjugated secondary antibodies for 1 hour at RT (1:500, Jackson ImmunoResearch). The slides were then washed in PBS and cell nuclei were stained with 4-6-diamidino-2-

phenylindole (DAPI). At the final step, the slides were mounted with Dako fluorescent Mounting Medium and images were visualized with a fluorescence microscope using Axiovision software (Carl Zeiss MicroImaging). To confirm the cellular localization of WT and mutant Cx32 in co-expressing cells, we also performed confocal microscopy using a Leica DMR microscope (Leica Microsystems).

For *quantification of GJ plaque formation* in transfected cells as an indication of Cx32 trafficking to the cell membrane, we counted the number of GJ plaques per cell in n=50 cells for each experiment/mutation where mutant and WT Cx32 were co-expressed, compared to the number of GJ plaques formed in cells expressing only the WT Cx32.

Immunoblot analysis

Protein samples were subjected to 10% SDS gel electrophoresis and transferred onto a PVDF membrane (GE Healthcare Life Sciences) by a wet transfer unit using 1x transfer buffer (25 mM Tris, 192 mM Glycine, 20% methanol). Non-specific sites were blocked with 5% skimmed milk powder diluted in 0.1% PBS-Tween 20 (PBS-T) for 1 hour at RT. Membranes were incubated at 4^{o}C overnight with rat anti-flag (1:500, Biolegend), mouse anti-myc (1:200, Cell Signaling) and mouse anti-β-tubulin (1:3000, Developmental Studies Hybridoma Bank). The following day, the membranes were washed 3x with PBS-T and were further incubated with anti-rat or anti-mouse secondary antibodies conjugated to horseradish peroxidise (HRP) (1:3000, Jackson ImmunoResearch) for 1 hour at RT. After washing, the bands were visualized using the enhanced chemiluminescence system (ECL, GE Healthcare Bio-Sciences). Band intensities were calculated using Tinascan software.

Immunoprecipitation assay

Co-transfected cells (with WT Cx32-flag tagged and mutant Cx32-myc tagged) were harvested in ice-cold RIPA containing protease inhibitors (Roche). After harvesting, the cells were passed through a 25-gauge needle twice and spinned down at high speed for 30 min. The supernatant was used for the immunoprecipitation assay. Rat anti-flag (3 µg, Biolegend) was mixed with Protein G-Dynabeads (Invitrogen) magnetic particles for 45 min to coat the particles. The anti-Rat IgG-coated particles were then incubated overnight at 4^{o}C with 1000 mg of whole cell lysate. The following day, the particles were isolated with a ceramic magnet and then washed with cold 0.2% PBS-Tween 20, re-suspended in SDS-PAGE sample buffer and analysed by immunoblot using the mouse myc antibody (1:500, Santa Cruz). *For quantification*, Cx32 band intensity for each mutant was measured with Tinascan software and compared to the band intensity of the positive control, expressed as ratio, from two independent experiments.

Scrape loading assay

In order to examine the functional consequences of co-expressing mutants with WT Cx32 using the scrape loading method, we used an expression vector with dsRED as a reporter gene specifically for the mutants. The *GJB1*/Cx32 mutations T55I and M93V were excised from the pREP9 vector by double digestion with the BamHI and KpnI enzymes and were directionally cloned into the PSLN1180 plasmid. The entire ORF of the *GJB1*/Cx32 mutations was subsequently taken out by double digestion with the AgeI and EcoRI enzymes and cloned into the PQCXIX plasmid precisely upstream of the IRES.dsRED sequence. The *GJB1*/Cx32 mutations R75W and N175D were PCR amplified from previously used constructs using specifically designed primers that introduced the AgeI and EcoRI restriction sites (Primer #1: 5'- AAA CCG GTG GCA GGA TGA ACT GGA CAGG -3' and Primer #2: 5'- CCG GAA TTC CGG TTA CAG GTC CTC CT-3'). The PCR products were then digested and cloned into the PQCXIX plasmid, following digestion with the AgeI and EcoRI restriction endonucleases. Correct

assembly of the expression cassettes was confirmed by direct sequencing of the *GJB1* ORF for all constructs.

HeLa cells expressing the WT Cx32 after infection with the LV.*PGK*-*GJB1*.eGFP vector, were seeded on 6-well plates to reach approximately 70% confluency when transfected with the selected Cx32 mutants and about 90-100% confluency on the day of the scrape loading. In this experiment, cells were gently rinsed 3x with PBS without calcium or magnesium and incubated with Lucifer yellow fluorescent stain (Sigma, MW: 457.25), a molecule that is transferred through GJs, diluted in PBS at a final concentration 100µM. Immediately after the addition of Lucifer yellow, cells were scraped drawing horizontal and vertical lines using a scalpel blade and incubated in the dark for 10 minutes. Afterwards, cells were washed 3x with Hank´s Balanced Salt Solution (HBSS) containing calcium and magnesium to stop GJ communication and coverslips were used to cover the cells. Pictures were captured using a Nikon Eclipse TE2000-U microscope with a Nikon digital Camera DXM 1200F.

To *quantify the formation of functional GJ channels*, we counted the number of coupled cells co-expressing the WT and mutant Cx32 that were also positive for the Lucifer yellow fluorescence (excluding cells on the scrape line), indicating dye transfer through GJs from neighboring cells. For each mutation n=20 cells were counted from 3 independent experiments. The results were expressed as percentage of coupled cells compared to the positive control experiment where cells expressed the WT Cx32 only.

Experimental animals

Two month-old C57BL/6 male and female mice expressing on a *Gjb1*-null background either the T55I (T55I KO) (n=8) or the R75W mutation (R75W KO) (n=4) described elsewhere (12) were used for intraneural injections of the WT *GJB1* gene cloned into a lentiviral vector, as previously

described (30). Mice were injected in the sciatic nerve with the mock vector on one side and with the full vector on the contralateral side. All experimental procedures were conducted in agreement with animal care protocols approved by the Cyprus Government's Chief Veterinary Officer and according to EU guidelines (EC Directive 86/609/EEC).

Intraneural Injection of the Lentiviral Vector

The mice were initially anesthetized and surgically incised close to the sciatic nerve area to gain access to the nerve. Pulled glass micropipettes were used to inject the nerve immediately distal to the sciatic notch using a microinjector (FemtoJet; Eppendorf, Hamburg, Germany). For each nerve, ten microliters of either full or mock vector were injected and 5/0 silk suture (Silkam; Braun, Melsungen, Germany) was used promptly to close the wounds. Mice were sacrificed 4 weeks after gene delivery and the expression of Cx32 was examined by immunostaining of teased nerve fibers. The lentiviral stock titers were between 3.6×10^{11} (full vector) and 4×10^{12} (mock vector) viral particles/ml.

Immunohistochemistry

For immunofluorescence staining of sciatic nerve teased fibers, mice were firstly anesthetized with Avertin in accordance to approved protocols and transcardially perfused with saline solution (NaCl 0.9%) followed by 4% PFA diluted in 0.1 M Phospate buffer (PB). The bilateral sciatic nerves were detached from the knee to the spinal cord and divided into proximal, middle and distal segments. All segments were teased under a stereoscope and teased fibers were transferred onto slides, air dried overnight and frozen at -20^{o}C until used. Teased fibers were permeabilized in acetone for 10 min at -20^{o}C and washed 3x in PBS, then blocked in blocking solution (5% BSA with 0.5% Triton-X) for 1 hour at RT. Primary antibodies were added and incubated overnight at 4^{o}C, including rabbit anti-Cx32 (1:50, Sigma-Aldrich) and mouse anti-Caspr (1:100, gift from Prof. Steven Scherer, University of Pennsylvania). The following day, the slides were

washed in PBS and incubated with fluorescein- and rhodamine-conjugated secondary antibodies for 1 hour at RT (1:500, Jackson ImmunoResearch). Cell nuclei were stained with DAPI and slides were mounted with Dako fluorescent Mounting Medium. Images were captured with a fluorescence microscope using Axiovision software (Carl Zeiss MicroImaging).

Quantification of Cx32 positive nodal areas (defined as the ones showing Cx32 immunoreactivity in paranodal myelin areas) out of 50 randomly selected nodes was performed in multiple teased fiber preparations from all mice that received the full vector and statistical analysis was conducted by comparing the number of Cx32-positive nodes in the T55I KO and R75W KO nerves to the number of positive nodes in simple Cx32 KO mice.

Statistical analysis

All statistical comparisons were performed using the unpaired two-sided Student's t-test and Microsoft Excel software (Microsoft, Redmond, WA). Values were presented as mean ± standard deviation (SD). A value of $p<0.05$ was considered statistically significant.

Acknowledgements

This work was supported by the Muscular Dystrophy Association (grant MDA 277250 to KAK). Styliana Kyriakoudi was supported by a Hellenic Bank Scholarship through the Cyprus School of Molecular Medicine. We thank Panayiota Pirpa and Dr. Andreas Hadjisavvas for technical assistance with sequencing mutant constructs, as well as Dr. Jan Richter for technical assistance with the production of lentiviral vectors. We also thank Dr Nikolas Mastroyiannopoulos for his assistance with microscopy and Neoklis Makrides for help with confocal imaging.

The monoclonal antibody anti-β-tubulin (developed by Michael Klymkowsky) was obtained from the Developmental Studies Hybridoma Bank developed under the auspices of the National Institute of Child Health and Human Development and maintained by Department of Biology, The University of Iowa, Iowa City.

Conflict of interest: There is no conflict of interest.

References

1 Herringham, W.P. (1888) Muscular atrophy of the peroneal type affecting many members of a family. *Brain*, **11**, 230-236.

2 Bergoffen, J., Scherer, S.S., Wang, S., Scott, M.O., Bone, L.J., Paul, D.L., Chen, K., Lensch, M.W., Chance, P.F. and Fischbeck, K.H. (1993) Connexin mutations in X-linked Charcot-Marie-Tooth disease. *Science*, **262**, 2039-2042.

3 Kleopa, K.A. and Scherer, S.S. (2006) Molecular genetics of X-linked Charcot-Marie-Tooth disease. *Neuromolecular Med.*, **8**, 107-122.

4 Scherer, S.S., Deschenes, S.M., Xu, Y.T., Grinspan, J.B., Fischbeck, K.H. and Paul, D.L. (1995) Connexin32 is a myelin-related protein in the PNS and CNS. *J. Neurosci.*, **15**, 8281-8294.

5 Bruzzone, R., White, T.W. and Paul, D.L. (1996) Connections with connexins: the molecular basis of direct intercellular signaling. *Eur. J. Biochem.*, **238**, 1-27.

6 Goodenough, D.A., Goliger, J.A. and Paul, D.L. (1996) Connexins, connexons, and intercellular communication. *Annu. Rev. Biochem.*, **65**, 475-502.

7 Berger, P., Niemann, A. and Suter, U. (2006) Schwann cells and the pathogenesis of inherited motor and sensory neuropathies (Charcot-Marie-Tooth disease). *Glia*, **54**, 243-257.

8 Scherer, S.S. (1997) The biology and pathobiology of Schwann cells. *Curr. Opin. Neurol.*, **10**, 386-397.

9 Pareyson, D. and Marchesi, C. (2009) Diagnosis, natural history, and management of Charcot-Marie-Tooth disease. *Lancet Neurol.*, **8**, 654-667.

10 Jani-Acsadi, A., Krajewski, K. and Shy, M.E. (2008) Charcot-Marie-Tooth neuropathies: diagnosis and management. *Semin. Neurol.*, **28**, 185-194.

11 Bruzzone, R., White, T.W., Scherer, S.S., Fischbeck, K.H. and Paul, D.L. (1994) Null mutations of connexin32 in patients with X-linked Charcot-Marie-Tooth disease. *Neuron*, **13**, 1253-1260.

12 Sargiannidou, I., Vavlitou, N., Aristodemou, S., Hadjisavvas, A., Kyriacou, K., Scherer, S.S. and Kleopa, K.A. (2009) Connexin32 mutations cause loss of function in Schwann cells and oligodendrocytes leading to PNS and CNS myelination defects. *J. Neurosci.*, **29**, 4736-4749.

13 Shy, M.E., Siskind, C., Swan, E.R., Krajewski, K.M., Doherty, T., Fuerst, D.R., Ainsworth, P.J., Lewis, R.A., Scherer, S.S. and Hahn, A.F. (2007) CMT1X phenotypes represent loss of GJB1 gene function. *Neurology*, **68**, 849-855.

14 Scherer, S.S., Xu, Y.T., Nelles, E., Fischbeck, K., Willecke, K. and Bone, L.J. (1998) Connexin32-null mice develop demyelinating peripheral neuropathy. *Glia*, **24**, 8-20.

15 Anzini, P., Neuberg, D.H., Schachner, M., Nelles, E., Willecke, K., Zielasek, J., Toyka, K.V., Suter, U. and Martini, R. (1997) Structural abnormalities and deficient maintenance of peripheral nerve myelin in mice lacking the gap junction protein connexin 32. *J. Neurosci.*, **17**, 4545-4551.

16 Deschenes, S.M., Walcott, J.L., Wexler, T.L., Scherer, S.S. and Fischbeck, K.H. (1997) Altered trafficking of mutant connexin32. *J. Neurosci.*, **17**, 9077-9084.

17 Omori, Y., Mesnil, M. and Yamasaki, H. (1996) Connexin 32 mutations from X-linked Charcot-Marie-Tooth disease patients: functional defects and dominant negative effects. *Mol. Biol. Cell*, **7**, 907-916.

18 Martin, P.E., Mambetisaeva, E.T., Archer, D.A., George, C.H. and Evans, W.H. (2000) Analysis of gap junction assembly using mutated connexins detected in Charcot-Marie-Tooth X-linked disease. *J. Neurochem.*, **74**, 711-720.

19 Kleopa, K.A., Yum, S.W. and Scherer, S.S. (2002) Cellular mechanisms of connexin32 mutations associated with CNS manifestations. *J. Neurosci. Res.*, **68**, 522-534.

20 Yum, S.W., Kleopa, K.A., Shumas, S. and Scherer, S.S. (2002) Diverse trafficking abnormalities of connexin32 mutants causing CMTX. *Neurobiol. Dis.*, **11**, 43-52.

21 VanSlyke, J.K., Deschenes, S.M. and Musil, L.S. (2000) Intracellular transport, assembly, and degradation of wild-type and disease-linked mutant gap junction proteins. *Mol. Biol. Cell*, **11**, 1933-1946.

22 Castro, C., Gomez-Hernandez, J.M., Silander, K. and Barrio, L.C. (1999) Altered formation of hemichannels and gap junction channels caused by C-terminal connexin-32 mutations. *J. Neurosci.*, **19**, 3752-3760.

23 Oh, S., Ri, Y., Bennett, M.V., Trexler, E.B., Verselis, V.K. and Bargiello, T.A. (1997) Changes in permeability caused by connexin 32 mutations underlie X-linked Charcot-Marie-Tooth disease. *Neuron*, **19**, 927-938.

24 Ressot, C., Gomes, D., Dautigny, A., Pham-Dinh, D. and Bruzzone, R. (1998) Connexin32 mutations associated with X-linked Charcot-Marie-Tooth disease show two distinct behaviors: loss of function and altered gating properties. *J. Neurosci.*, **18**, 4063-4075.

25 Hahn, A.F., Ainsworth, P.J., Bolton, C.F., Bilbao, J.M. and Vallat, J.M. (2001) Pathological findings in the x-linked form of Charcot-Marie-Tooth disease: a morphometric and ultrastructural analysis. *Acta Neuropathol.*, **101**, 129-139.

26 Vavlitou, N., Sargiannidou, I., Markoullis, K., Kyriacou, K., Scherer, S.S. and Kleopa, K.A. (2010) Axonal pathology precedes demyelination in a mouse model of X-linked demyelinating/type I Charcot-Marie Tooth neuropathy. *J. Neuropathol. Exp. Neurol.*, **69**, 945-958.

27 Senderek, J., Hermanns, B., Bergmann, C., Boroojerdi, B., Bajbouj, M., Hungs, M., Ramaekers, V.T., Quasthoff, S., Karch, D. and Schroder, J.M. (1999) X-linked dominant Charcot-Marie-Tooth neuropathy: clinical, electrophysiological, and morphological phenotype in four families with different connexin32 mutations. *J. Neurol. Sci.*, **167**, 90-101.

28 Kleopa, K.A. (2011) The role of gap junctions in Charcot-Marie-Tooth disease. *J. Neurosci.*, **31**, 17753-17760.

29 Jeng, L.J., Balice-Gordon, R.J., Messing, A., Fischbeck, K.H. and Scherer, S.S. (2006) The effects of a dominant connexin32 mutant in myelinating Schwann cells. *Mol. Cell. Neurosci.*, **32**, 283-298.

30 Sargiannidou, I., Kagiava, A., Bashiardes, S., Richter, J., Christodoulou, C., Scherer, S.S. and Kleopa, K.A. (2015) Intraneural GJB1 gene delivery improves nerve pathology in a model of X-linked Charcot-Marie-Tooth disease. *Ann. Neurol.*, **78**, 303-316.

31 Kagiava, A., Sargiannidou, I., Theophilidis, G., Karaiskos, C., Richter, J., Bashiardes, S., Schiza, N., Nearchou, M., Christodoulou, C., Scherer, S.S. *et al.* (2016) Intrathecal gene therapy rescues a model of demyelinating peripheral neuropathy. *Proc. Natl. Acad. Sci. U S A*, **113**, 28.

32 Kleopa, K.A., Zamba-Papanicolaou, E., Alevra, X., Nicolaou, P., Georgiou, D.M., Hadjisavvas, A., Kyriakides, T. and Christodoulou, K. (2006) Phenotypic and cellular expression of two novel connexin32 mutations causing CMT1X. *Neurology*, **66**, 396-402.

33 Segretain, D. and Falk, M.M. (2004) Regulation of connexin biosynthesis, assembly, gap junction formation, and removal. *Biochim. Biophys. Acta*, **23**, 1-2.

34 Laird, D.W. (2006) Life cycle of connexins in health and disease. *Biochem. J.*, **394**, 527-543.

35 Scherer, S.S., Xu, Y.T., Messing, A., Willecke, K., Fischbeck, K.H. and Jeng, L.J. (2005) Transgenic expression of human connexin32 in myelinating Schwann cells prevents demyelination in connexin32-null mice. *J. Neurosci.*, **25**, 1550-1559.

36 Hoseki, J., Ushioda, R. and Nagata, K. (2010) Mechanism and components of endoplasmic reticulum-associated degradation. *J. Biochem.*, **147**, 19-25.

37 Falk, M.M. (2000) Biosynthesis and structural composition of gap junction intercellular membrane channels. *Eur. J. Cell Biol.*, **79**, 564-574.

38 Smith, T.D., Mohankumar, A., Minogue, P.J., Beyer, E.C., Berthoud, V.M. and Koval, M. (2012) Cytoplasmic amino acids within the membrane interface region influence connexin oligomerization. *J. Membr. Biol.*, **245**, 221-230.

39 Maza, J., Das Sarma, J. and Koval, M. (2005) Defining a minimal motif required to prevent connexin oligomerization in the endoplasmic reticulum. *J. Biol. Chem.*, **280**, 21115-21121.

40 Abrams, C.K., Freidin, M.M., Verselis, V.K., Bennett, M.V. and Bargiello, T.A. (2001) Functional alterations in gap junction channels formed by mutant forms of connexin 32: evidence for loss of function as a pathogenic mechanism in the X-linked form of Charcot-Marie-Tooth disease. *Brain Res.*, **900**, 9-25.

41 Wang, H.L., Chang, W.T., Yeh, T.H., Wu, T., Chen, M.S. and Wu, C.Y. (2004) Functional analysis of connexin-32 mutants associated with X-linked dominant Charcot-Marie-Tooth disease. *Neurobiol. Dis.*, **15**, 361-370.

42 Komor, A.C., Badran, A.H. and Liu, D.R. (2016) CRISPR-Based Technologies for the Manipulation of Eukaryotic Genomes. *Cell*, **15**, 31465-31469.

43 Aigner, A. (2006) Gene silencing through RNA interference (RNAi) in vivo: strategies based on the direct application of siRNAs. *J. Biotechnol.*, **124**, 12-25.

44 Miller, V.M., Xia, H., Marrs, G.L., Gouvion, C.M., Lee, G., Davidson, B.L. and Paulson, H.L. (2003) Allele-specific silencing of dominant disease genes. *Proc. Natl. Acad. Sci. U S A*, **100**, 7195-7200.

45 Hohjoh, H. (2013) Disease-causing allele-specific silencing by RNA interference. *Pharmaceuticals*, **6**, 522-535.

Figure legends

Figure 1: Co-expression of WT Cx32 with CMT1X mutants. Images of immunostained HeLa cells co-expressing the flag-tagged wild type (WT) Cx32 along with each of the myc-tagged A39P, A39V, T55I, R75W, M93V, L143P, N175D and R183S mutants as indicated (**A-H**) or the myc-tagged WT protein as control (**I**). Anti-myc antibody (green) recognizes mutant Cx32, whereas anti-flag antibody (red) recognizes WT Cx32. Cell nuclei are counterstained with DAPI (blue). Most mutants show intracellular localization, either exclusively, or with additional membrane expression and gap junction (GJ) plaque formation (M93V, R183S). The co-expressed WT Cx32 shows variable cellular localization and GJ formation on the cell membrane. In the presence of the ER-retained A39P, A39V and T55I mutants (**A-C**) WT Cx32 appears to form normally GJ plaques (open arrowheads) and shows no intracellular immunoreactivity. In the presence of Golgi-retained mutants WT Cx32 shows intracellular retention and reduced GJ formation, most prominently with co-expressed R75W mutant (**D**), but also with M93V, L143P and N175D mutants (**E-G**). In cells co-expressing mutants that reach the cell membrane (M93V, R183S) WT Cx32 and mutant Cx32 are partly co-localized in GJ-like plaques (**E, H**). **J**: Quantification of GJ plaque formation by the WT protein (number of membrane GJ plaques per cell) in n=50 cells for each co-expressed mutant revealed that the R75W and N175D mutants significantly reduce the correct trafficking of the WT Cx32 to the cell surface ($p<0.001$ and $p=0.00608$, respectively) as compared to the number of GJ plaques formed by the WT Cx32 alone. The remaining five mutants did not cause significant changes in this experiment. ***$p<0.001$, **$p<0.01$, Scale bar=10 μm.

Figure 2: Immunoblot analysis demonstrating the expression levels of mutant and WT Cx32 in HeLa cells. Lysates of HeLa cells transiently co-transfected to express each of the myc-tagged

Cx32 mutants as indicated along with the flag-tagged WT Cx32, were immunoblotted using antibodies recognizing the myc or flag tags on the proteins. An empty plasmid was also co-transfected with the flag-tagged WT Cx32 as a negative control for the myc antibody. Note the absence of any bands in untransfected HeLa cells in the first lane, which was used as a negative control. Tubulin blot is shown below as a loading control. The expression levels of most mutants were similar to WT Cx32 with some also showing lower or higher levels compared to the WT protein, as indicated by the intensity of myc and flag bands, respectively.

Figure 3: Some of the Golgi-retained CMT1X mutants interact directly with the WT Cx32. Co-immunoprecipitation (co-IP) of the flag-tagged WT Cx32 protein co-expressed in HeLa cells with myc-tagged Cx32 mutants as indicated using a flag antibody followed by immunoblot with a myc antibody to assess the interactions between the WT and mutant proteins (**A**). HeLa cells expressing the flag-tagged WT protein only, served as a negative control. The co-expression of the myc and flag-tagged WT proteins (WT+WT) served as a positive control for the experiment. Five of the mutants showed no co-IP with the WT protein, while the Golgi-retained R75W, M93V and N175D mutants revealed a partial interaction, as compared to the positive control. The results of the N175D mutant are from a different gel. Quantification of band intensity reflecting the percentage of mutant-WT compared to WT-WT (considered as 100%) direct interaction from two independent experiments is shown in (**B**).

Figure 4: Impaired WT Cx32 GJ channel function in cells co-expressing the R75W, M93V and N175D **but not the T55I mutant.** These are representative immunofluorescence images of scrape-loaded (with Lucifer yellow) HeLa cells that co-express the WT Cx32 along with the T55I (**A-D**), R75W (**E-H**), M93V (**I-L**) or the N175D (**M-P**) mutants. Panels A, E, I and M show the

cells expressing the WT Cx32 indicated by GFP green fluorescence, panels B, F, J and N show the cells expressing the mutants indicated by dsRed red fluorescence, while panels C,G, K and O show cells that contain Lucifer yellow. Overlap images are shown in Panels D, H, L and P. In cells co-expressing the T55I mutant and the WT Cx32, Lucifer yellow diffuses into adjacent cells (white arrows), demonstrating that cellular GJ connectivity is not abolished. In contrast, cells co-expressing WT Cx32 and the R75W, M93V or the N175D mutant show reduced dye transfer to adjacent cells indicating impaired formation of functional GJs. **Q**: Quantification of cellular GJ connectivity (% of mutant-WT Cx32 double expressing cells showing dye transfer to adjacent cells from n=20 double expressing cells in each experiment) shows significant reduction of coupled cells in the presence of the R75W (66.7±2.9% coupled cells, p=0.0001), M93V (76.7±2.9% coupled cells, p=0.00055) and N175D (73.3±7.6% coupled cells, p=0.0063) mutants but not in the presence of the T55I mutant (88.3±5.8%, p>0.05) compared to cells expressing WT Cx32 alone (97.3±2.1%). Scale bar=20µm.

Figure 5: The Golgi-retained R75W mutant but not the ER-retained T55I mutant interferes with the expression of virally delivered WT Cx32 *in vivo*. These are images from sciatic nerve teased fibers of LV.*Mpz*-eGFP (mock) vector injected T55I KO nerves as negative control (**A**), as well as LV.*Mpz-GJB1* (full) vector injected T55I KO (**B**) or R75W KO (**C**) nerves, immunostained with antibodies to Cx32 (red) and paranodal marker Caspr (green). Cell nuclei are stained with DAPI (blue). In the higher magnification images, asterisks indicate Schwann cell nuclei showing also the cytoplasmic/perinuclear expression of the retained T55I and R75W mutants (red). WT Cx32 immunoreactivity is normally localized in the paranodal areas of non-compact myelin in the T55I KO mice (arrows in B) but not in the R75W KO nerve fibers (C) or in mock injected T55I KO nerves (A). **D**: Quantification of nodal myelin areas expressing Cx32 shows similar rates of paranodal localization of virally delivered WT Cx32 in T55I KO fibers

(34±7.6% Cx32-positive paranodal areas, p>0.05) compared to Cx32 KO (*Gjb1*-/-) (36±5.5%), whereas in most R75W KO fibers injected with the full vector WT Cx32 does not reach the paranodal areas (10±2.3%, p=0.00011). Scale bar=30 μm.

Supplementary figures

Supplementary Figure 1: Cellular expression of CMT1X mutants co-localizing with cell markers. These are representative immunofluorescence images of transfected HeLa cells expressing different Cx32 mutants as indicated, double immunostained for Cx32 (red) and either the endoplasmic reticulum (ER) marker calnexin (**A-C**) or the Golgi marker 58k (**D-H**) (both in green) as indicated, to clarify the intracellular localization of each mutant. Cell nuclei are counterstained with DAPI (blue). The A39P, A39V and T55I mutants are co-localized with the ER marker calnexin, whereas the R75W, M93V, L143P, N175D and R183S mutants are mostly co-localized with the Golgi marker 58k. Scale bar=10 μm.

Supplementary Figure 2: Cellular expression of CMT1X mutants. These are immunofluorescence images of transfected HeLa cells expressing different Cx32 mutants as indicated, double immunostained for Cx32 (red) and either the Golgi marker 58k (**A-C**) or the ER marker calnexin (**D-H**) (both in green) as indicated, to clarify the intracellular localization of each mutant. Cell nuclei are counterstained with DAPI (blue). The A39P, A39V and T55I mutants do not colocalize with the Golgi marker 58k, while the R75W, M93V, L143P, N175D and R183S mutants are mostly restricted to the Golgi compartment and do not co-localize with the ER marker calnexin. Scale bar=10 μm.

Supplementary Figure 3: CMT1X mutants show complete or partial intracellular retention. These are immunofluorescence images of HeLa cells expressing Cx32 mutants (**A-H**) or the WT protein (**I**) as indicated, immunostained with the membrane marker cadherin (green) and Cx32

(red). Cell nuclei are counterstained with DAPI (blue). All mutants (A-H) are retained intracellularly as most of their immunoreactivity is inside of the cadherin immunoreactivity which marks the cell membrane without co-localization, in contrast to the WT protein which is mostly co-localized with cadherin on the cell membrane forming GJ plaques (I). However, some of the mutants show additional localization on the cell membrane, including the M93V and R183S (open arrowheads). Scale bar=10 μm.

Supplementary Figure 4: Confocal analysis of co-expressed WT Cx32 with CMT1X mutants. These are confocal images of immunostained HeLa cells co-expressing the flag-tagged wild type (WT) Cx32 along with each of the myc-tagged A39P, A39V, T55I, R75W, M93V, L143P, N175D and R183S mutants as indicated (**A-H**)**.** Anti-myc antibody (green) recognizes mutant Cx32, whereas anti-flag antibody (red) recognizes WT Cx32. In the presence of the ER-retained A39P, A39V and T55I mutants (**A-C**) WT Cx32 appears to form normally GJ plaques (open arrowheads) and shows no intracellular immunoreactivity. In the presence of Golgi-retained mutants, WT Cx32 shows intracellular retention and reduced GJ formation, most prominently with co-expressed R75W mutant (**D**), but also with M93V, L143P and N175D mutants (**E-G**). In cells co-expressing mutants with intracellular localization that also reach the cell membrane (M93V, R183S), WT and mutant Cx32 are partly co-localized in GJ-like plaques (**E, H**). Scale bar=2 μm.

Table 1: Cx32 mutants studied and *in vitro* cellular expression pattern

Mutation	**Cellular localization**	**Gap junctions formed**	**Previous studies**
A39P (c.115 G>C)	Endoplasmic reticulum	None	(19)
A39V (c.116 C>T)	Endoplasmic reticulum	None	(19)
T55I (c.164 C>T)	Endoplasmic reticulum	None	(19)
R75W (c.223 C>T)	Golgi	None	(20)
M93V (c.277 A>G)	Golgi	Many	(19)
L143P (c.428 T>C)	Golgi	None	(32)
N175D (c.523 A>G)	Golgi	None	unpublished
R183S (c.547 C>A)	Golgi	Some	(19)

Table 2: Polymerase Chain Reaction (PCR) Primers Used for Site-Directed Mutagenesis

Mutation	**Primers***
M93V	Sense: 5'-CTCTCCTCGTGGCCGTGCACGTGGCTCAC -3' Antisense: 5'-GTGAGCCACGTGCACGGCCACGAGGAGAG – 3'
A39V	Sense: 5'-CATGGTGCTGGTGGTGGTTGCAGAGAGTGTGTGGG –3' Antisense:5'-CCCACACACTCTCTGCAACCACCACCAGCACCATG -3'
A39P	Sense: 5'-CATGGTGCTGGTGGTGCCTGCAGAGAGTGTGTG-3' Antisense: 5'-CACACACTCTCTGCAGGCACCACCAGCACCATG-3'
R183S	Sense: 5'-GGACTGCTTCGTGTCCAGCCCCACCGAGAAAAC-3' Antisense: 5'-GTTTTCTCGGTGGGGCTGGACACGAAGCAGTCC –3'
L143P	Sense: 5'-CGTGGTGTTCCGGCCGTTGTTTGAGGCCG –3' Antisense: 5'-CGGCCTCAAACAACGGCCGGAACACCACG -3'

*The highlighted base is the one altered in the underlined codon

Abbreviations

BSA: Bovine serum albumin

CMT: Charcot–Marie–Tooth disease

CMT1X: X-linked form of Charcot–Marie–Tooth disease type 1

Cx32: Connexin 32

DAPI: 4-6-diamidino-2-phenylindole

eGFP: Enhanced green fluorescent protein

GJ: Gap junction

GJB1: Gap junction beta-1 (gene)

ER: Endoplasmic reticulum

KO: Knockout

PBS: Phosphate buffered saline

PFA: Paraformaldehyde

SDS: Sodium dodecyl sulphate

WT: Wild type

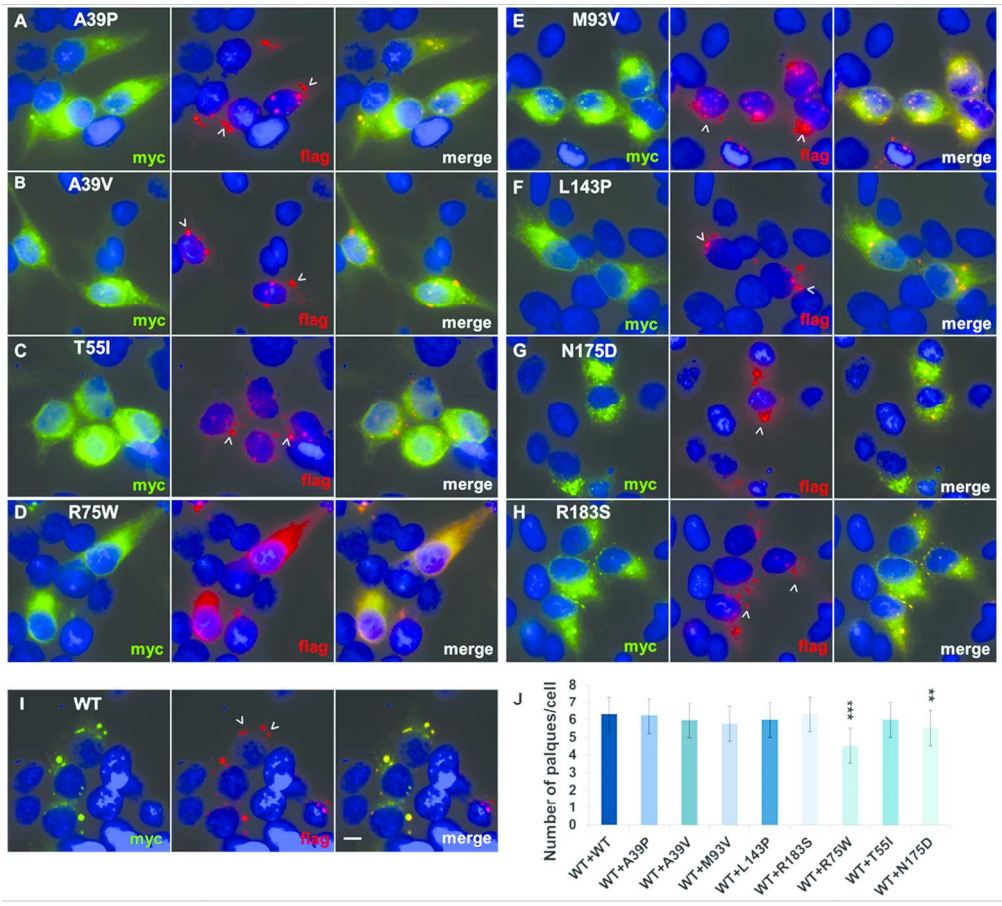

Figure 1: Co-expression of WT Cx32 with CMT1X mutants. Images of immunostained HeLa cells co-expressing the flag-tagged wild type (WT) Cx32 along with each of the myc-tagged A39P, A39V, T55I, R75W, M93V, L143P, N175D and R183S mutants as indicated (A-H) or the myc-tagged WT protein as control (I). Anti-myc antibody (green) recognizes mutant Cx32, whereas anti-flag antibody (red) recognizes WT Cx32. Cell nuclei are counterstained with DAPI (blue). Most mutants show intracellular localization, either exclusively, or with additional membrane expression and gap junction (GJ) plaque formation (M93V, R183S). The co-expressed WT Cx32 shows variable cellular localization and GJ formation on the cell membrane. In the presence of the ER-retained A39P, A39V and T55I mutants (A-C) WT Cx32 appears to form normally GJ plaques (open arrowheads) and shows no intracellular immunoreactivity. In the presence of Golgi-retained mutants WT Cx32 shows intracellular retention and reduced GJ formation, most prominently with co-expressed R75W mutant (D), but also with M93V, L143P and N175D mutants (E-G). In cells co-expressing mutants that reach the cell membrane (M93V, R183S) WT Cx32 and mutant Cx32 are partly co-localized in GJ-like plaques (E, H). J: Quantification of GJ plaque formation by the WT protein (number of membrane GJ plaques per cell) in n=50 cells for each co-expressed mutant revealed that the R75W and N175D mutants significantly reduce the correct trafficking of the WT Cx32 to the cell surface ($p<0.001$ and $p=0.00608$, respectively) as compared to the number of GJ plaques formed by the WT Cx32 alone. The remaining five mutants did not cause significant changes in this experiment. ***$p<0.001$, **$p<0.01$, Scale bar=10 μm.

Fig. 1
180x161mm (300 x 300 DPI)

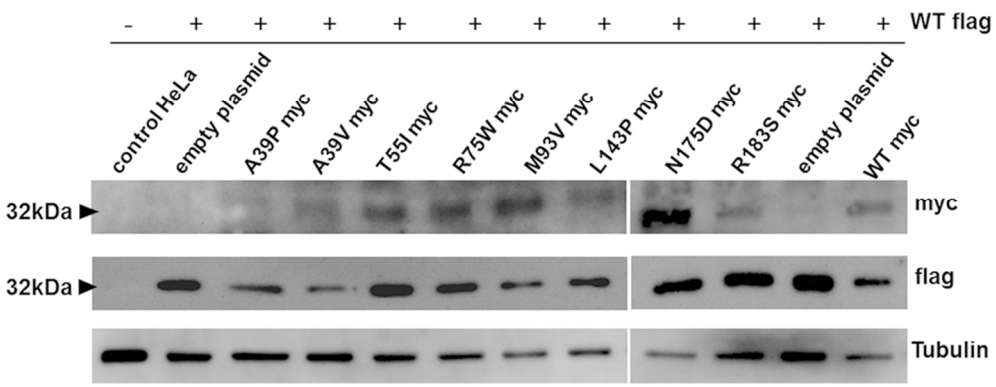

Figure 2: Immunoblot analysis demonstrating the expression levels of mutant and WT Cx32 in HeLa cells. Lysates of HeLa cells transiently co-transfected to express each of the myc tagged Cx32 mutants as indicated along with the flag tagged WT Cx32, were immunoblotted using antibodies recognizing the myc or flag tags on the proteins. An empty plasmid was also co-transfected with the flag tagged WT Cx32 as a negative control for the myc antibody. Note the absence of any bands in untransfected HeLa cells in the first lane, which was used as a negative control. Tubulin blot is shown below as a loading control. The expression levels of most mutants were similar to WT Cx32 with some also showing lower or higher levels compared to the WT protein, as indicated by the intensity of myc and flag bands, respectively.

Fig. 2

86x33mm (300 x 300 DPI)

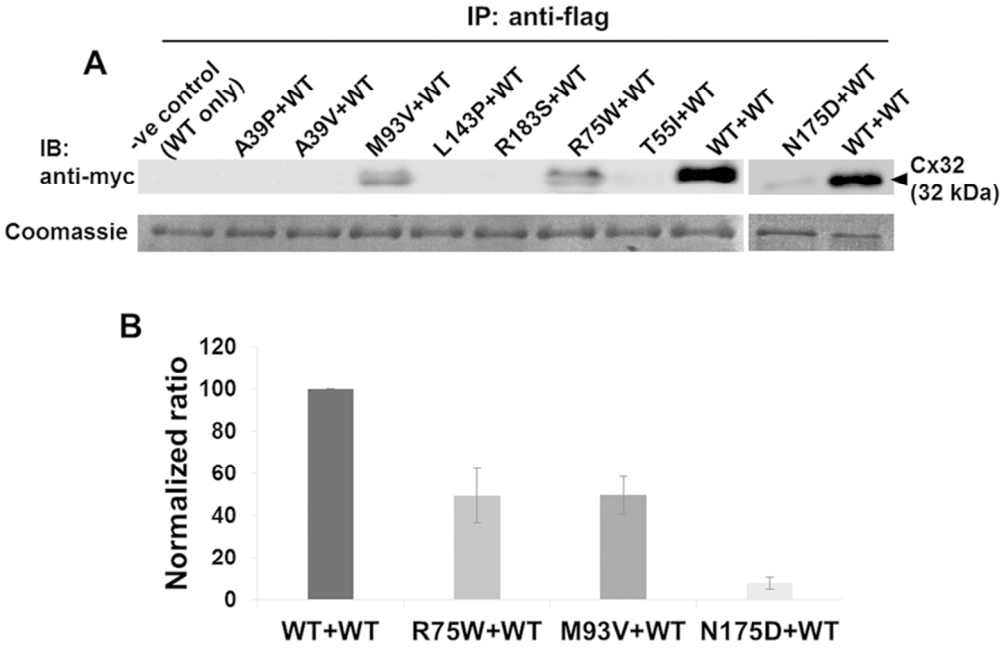

Figure 3: Some of the Golgi-retained CMT1X mutants interact directly with the WT Cx32. Co-immunoprecipitation (co-IP) of the flag-tagged WT Cx32 protein co-expressed in HeLa cells with myc-tagged Cx32 mutants as indicated using a flag antibody followed by immunoblot with a myc antibody to assess the interactions between the WT and mutant proteins (A). HeLa cells expressing the flag-tagged WT protein only, served as a negative control. The co-expression of the myc and flag-tagged WT proteins (WT+WT) served as a positive control for the experiment. Five of the mutants showed no co-IP with the WT protein, while the Golgi-retained R75W, M93V and N175D mutants revealed a partial interaction, as compared to the positive control. The results of the N175D mutant are from a different gel. Quantification of band intensity reflecting the percentage of mutant-WT compared to WT-WT (considered as 100%) direct interaction from two independent experiments is shown in (B).

Fig. 3

86x56mm (300 x 300 DPI)

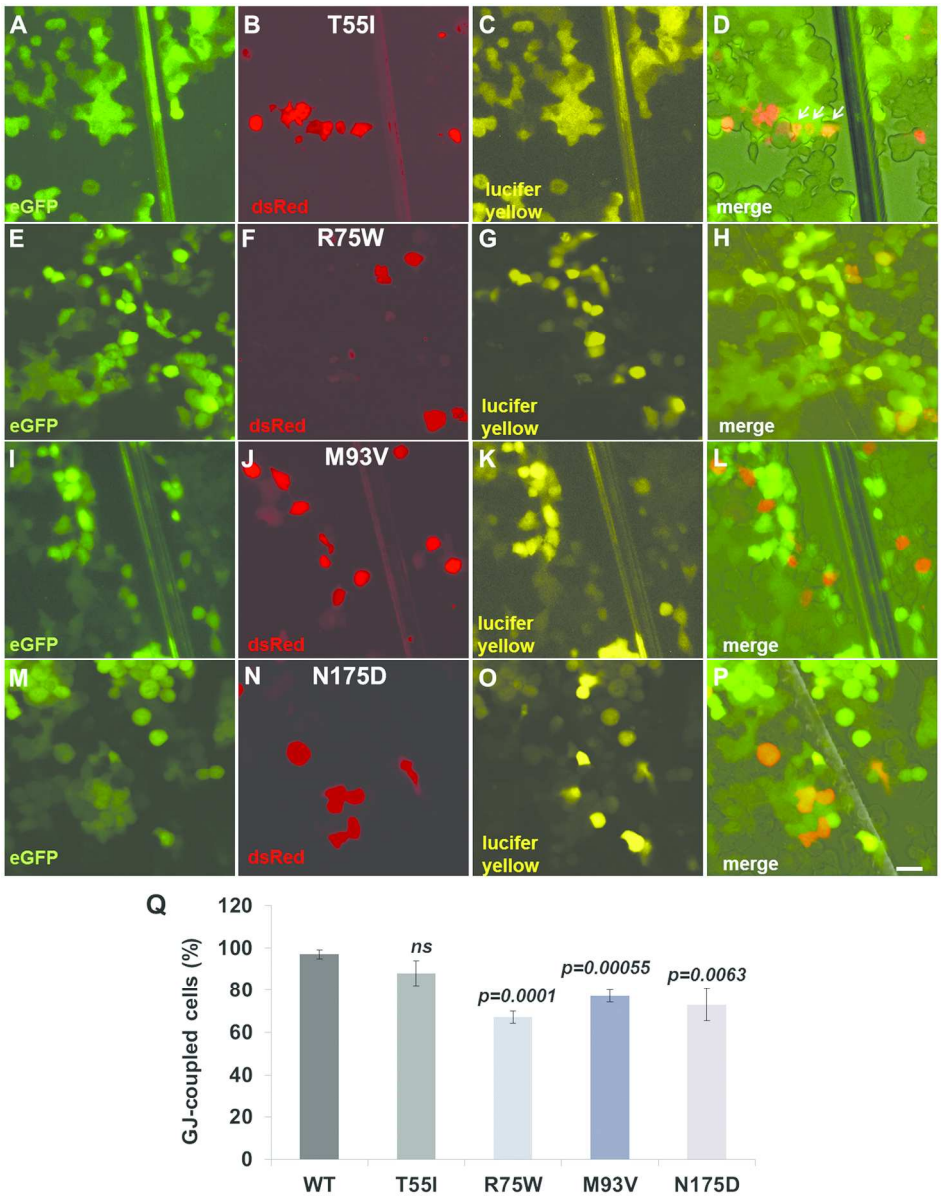

Figure 4: Impaired WT Cx32 GJ channel function in cells co-expressing the R75W, M93V and N175D but not the T55I mutant. These are representative immunofluorescence images of scrape-loaded (with Lucifer yellow) HeLa cells that co-express the WT Cx32 along with the T55I (A-D), R75W (E-H), M93V (I-L) or the N175D (M-P) mutants. Panels A, E, I and M show the cells expressing the WT Cx32 indicated by GFP green fluorescence, panels B, F, J and N show the cells expressing the mutants indicated by dsRed red fluorescence, while panels C,G, K and O show cells that contain Lucifer yellow. Overlap images are shown in Panels D, H, L and P. In cells co-expressing the T55I mutant and the WT Cx32, Lucifer yellow diffuses into adjacent cells (white arrows), demonstrating that cellular GJ connectivity is not abolished. In contrast, cells co-expressing WT Cx32 and the R75W, M93V or the N175D mutant show reduced dye transfer to adjacent cells indicating impaired formation of functional GJs. Q: Quantification of cellular GJ connectivity (% of mutant-WT Cx32 double expressing cells showing dye transfer to adjacent cells from n=20 double expressing cells in each experiment) shows significant reduction of coupled cells in the presence of the R75W (66.7±2.9% coupled cells, p=0.0001), M93V (76.7±2.9% coupled cells, p=0.00055) and N175D

(73.3±7.6% coupled cells, p=0.0063) mutants but not in the presence of the T55I mutant (88.3±5.8%, p>0.05) compared to cells expressing WT Cx32 alone (97.3±2.1%). Scale bar=20μm.

Fig. 4

180x229mm (300 x 300 DPI)

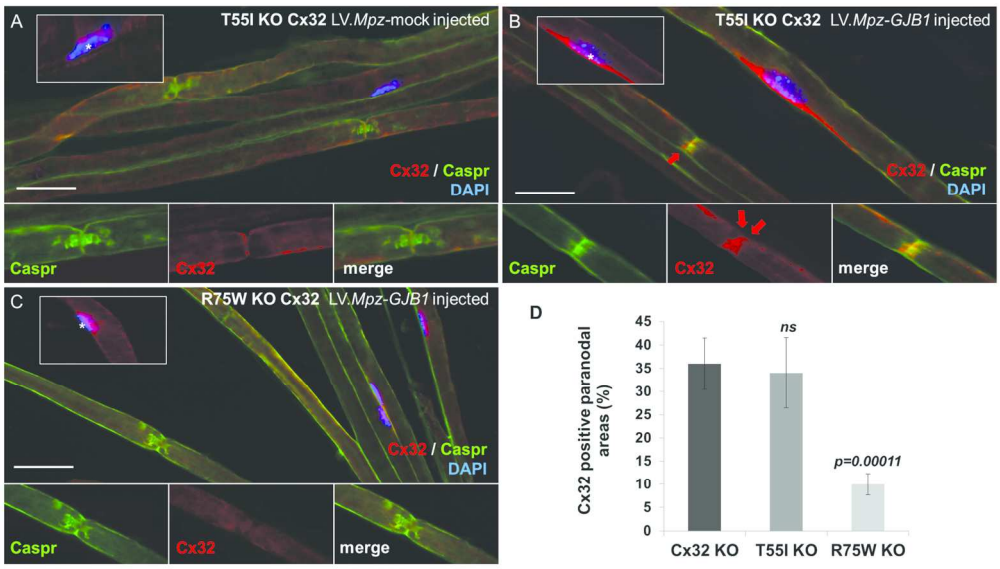

Figure 5: The Golgi-retained R75W mutant but not the ER-retained T55I mutant interferes with the expression of virally delivered WT Cx32 in vivo. These are images from sciatic nerve teased fibers of LV.Mpz.eGFP (mock) vector injected T55I KO nerves as negative control (A), as well as LV.Mpz.GJB1 (full) vector injected T55I KO (B) or R75W KO (C) nerves, immunostained with antibodies to Cx32 (red) and paranodal marker Caspr (green). Cell nuclei are stained with DAPI (blue). In the higher magnification images, asterisks indicate Schwann cell nuclei showing also the cytoplasmic/perinuclear expression of the retained T55I and R75W mutants (red). WT Cx32 immunoreactivity is normally localized in the paranodal areas of non-compact myelin in the T55I KO mice (arrows in B) but not in the R75W KO nerve fibers (C) or in mock-injected T55I KO nerves (A). D: Quantification of nodal myelin areas expressing Cx32 shows similar rates of paranodal localization of virally delivered WT Cx32 in T55I KO fibers (34±7.6% Cx32-positive paranodal areas, p>0.05) compared to Cx32 KO (Gjb1-/-) (36±5.5%), whereas in most R75W KO fibers injected with the full vector WT Cx32 does not reach the paranodal areas (10±2.3%, p=0.00011). Scale bar=30 μm.

Fig. 5
180x102mm (300 x 300 DPI)